Investigating the Role of Metal Chelation in HIV-1 Integrase Strand Transfer Inhibitors

ARTICLE *in* JOURNAL OF MEDICINAL CHEMISTRY · NOVEMBER 2011

Impact Factor: 5.45 · DOI: 10.1021/jm200851g · Source: PubMed

Journal of Medicinal Chemistry

Article

pubs.acs.org/jmc

Investigating the Role of Metal Chelation in HIV-1 Integrase Strand Transfer Inhibitors

Alessia Bacchi,[†] Mauro Carcelli,[†] Carlotta Compari,[‡] Emilia Fisicaro,[‡] Nicolino Pala,[§] Gabriele Rispoli,[†] Dominga Rogolino,*[,†] Tino W. Sanchez,[∥] Mario Sechi,[§] Valentina Sinisi,[†] and Nouri Neamati[∥]

[†]Dipartimento di Chimica Generale ed Inorganica, Chimica Analitica, Chimica Fisica and [‡]Dipartimento di Scienze Farmacologiche, Biologiche e Chimiche Applicate, Università di Parma, Parco Area delle Scienze 17/A, 43124 Parma, Italy

[§]Dipartimento di Scienze del Farmaco, Università di Sassari, Via Muroni 23/A, 07100 Sassari, Italy

[∥]Department of Pharmacology and Pharmaceutical Sciences, School of Pharmacy, University of Southern California, 1985 Zonal Avenue, Los Angeles, California 90089, United States

Supporting Information

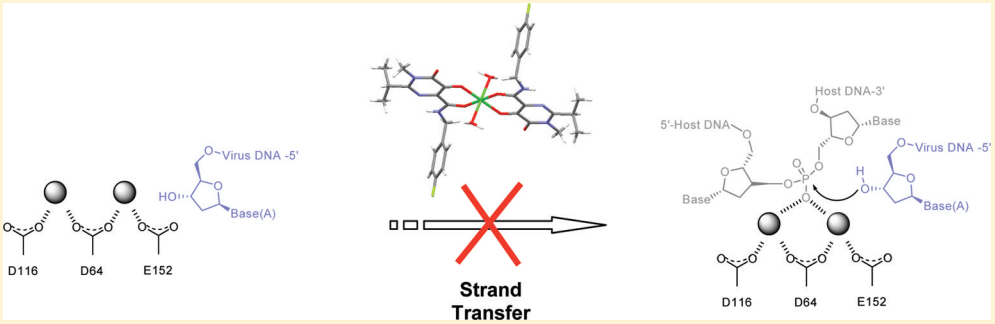

ABSTRACT: HIV-1 integrase (IN) has been validated as an attractive target for the treatment of HIV/AIDS. Several studies have confirmed that the metal binding function is a crucial feature in many of the reported IN inhibitors. To provide new insights on the metal chelating mechanism of IN inhibitors, we prepared a series of metal complexes of two ligands (HL^1 and HL^2), designed as representative models of the clinically used compounds raltegravir and elvitegravir. Potentiometric measurements were conducted for HL^2 in the presence of Mg(II), Mn(II), Co(II), and Zn(II) in order to delineate a metal speciation model. We also determined the X-ray structures of both of the ligands and of three representative metal complexes. Our results support the hypothesis that several selective strand transfer inhibitors preferentially chelate one cation in solution and that the metal complexes can interact with the active site of the enzyme.

INTRODUCTION

HIV-1 integrase (IN) is one of the three virally encoded enzymes responsible for the retroviral life cycle, together with protease and reverse transcriptase. IN catalyzes the integration of proviral cDNA into the host cell genome, a crucial step for viral replication.[1−3] Thus far, at least five IN inhibitors have been tested in HIV-infected patients[4,5] (Chart 1), and several others are under advanced preclinical and long-term toxicity studies. Raltegravir is the first IN inhibitor to be approved by the U.S. FDA.[6]

IN is composed of three domains: the C-terminal domain, responsible for nonspecific interaction with DNA; the N-terminal domain, containing a "zinc-binding motif" that is responsible for multimerization of the protein; the catalytic core domain. The last one is highly conserved among polymerases and polynucleotidyl transferases and comprises the so-called "D,D(35)E" motif, a triad of amino acids that coordinates two divalent metal ions,[7] probably Mg^{2+} ions.[8] The integration process promoted by IN consists of two distinct reactions: 3′-processing and strand transfer. In the first step the enzyme removes a terminal dinucleotide from the viral DNA, generating two CA-3′-hydroxyl recessed ends, which are the reactive intermediates required for the next step. The enzyme, still bound to the 3′-processed viral DNA, translocates to the nucleus of the infected cell as a part of the preintegration complex. Here the strand transfer step occurs, which consists of a trans-esterification reaction of the viral DNA 3′-OH on the phosphodiester backbone of the host DNA.

Magnesium ion is an essential cofactor in numerous enzymes such as polymerases, exonucleases, ribonucleases, transposases, and integrases and in many processes involving formation and modification of phosphate chains.[9] Understanding the mechanism of action of the inhibitors that act by chelating magnesium is therefore of great importance in order to develop new drugs not only against IN but also against other viral metalloenzymes (i.e., hepatitis C virus polymerase and influenza endonuclease).[9,10]

Received: June 30, 2011
Published: November 8, 2011

dx.doi.org/10.1021/jm200851g | J. Med. Chem. 2011, 54, 8407–8420

Chart 1. Selected DKA-Based and Representative HIV-1 Integrase Inhibitors

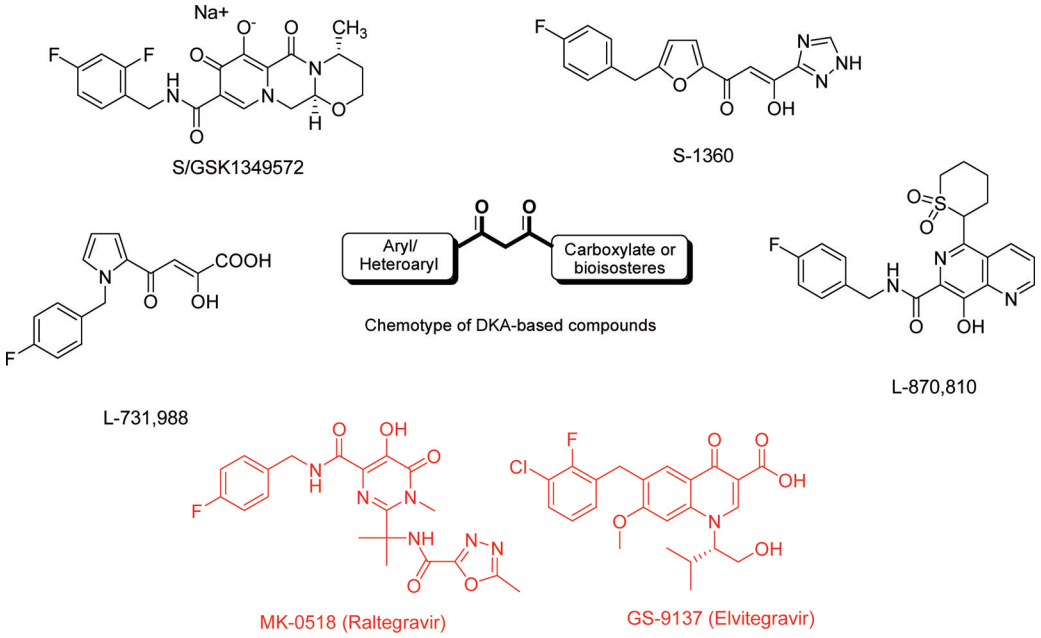

Previously, several potent IN inhibitors based on the β-diketo acids (DKAs) scaffold have been identified.[11−13] The general features of these inhibitors include a β-diketo moiety, an aromatic or heteroaromatic portion, and a carboxylic functionality (Chart 1). Several studies[14−16] have pointed out the importance of the hydrophobic part for activity, probably because it allows the correct accommodation of the molecule within the active site through a series of interactions with the protein side chain. The replacement of the keto−enolic moiety and/or of the carboxylic group with their bioisosteres led to other classes of inhibitors, such as the keto−enol triazoles (S-1360)[1−3,17,18] or the more recent naphthyridinecarboxamide (L-870,810),[19,20] hydroxypyrimidinecarboxamide (HPCA, MK-0518),[21−24] quinolone carboxylic acid (QCA, GS-9137),[25−28] and the pyridopyrazinooxazine derivatives (S/GSK1349572)[29] (Chart 1). Selective IN strand transfer inhibitors (SSTI) share a common scaffold that is able to chelate divalent metal ions, in accordance with the "two-metal binding model"[30] that emerged as an important strategy for the development of new IN inhibitors.[13,31] According to this model, the DKA-based pharmacophore is involved in the sequestration of the magnesium cofactors, preventing the interaction between the viral protein and the DNA substrate and thus blocking the enzymatic action at the strand transfer stage. The X-ray crystal structure of the full-length prototype foamy virus enzyme in complex with the viral DNA, in the absence and in the presence of inhibitors (raltegravir and elvitegravir), supports these considerations, since the drugs are located within the catalytic core with their chelating moieties oriented toward the metal ions.[32] The capability of the classical diketo acid motif to chelate two divalent metal ions at physiological conditions were elucidated by our[33,34] and other studies.[35] In particular, these studies suggested that DKA could act when complexed with a metal ion and not only as a free ligand.

In the more recent and active examples of SSTI, the DKA moiety was replaced by the hydroxypyrimidone ring conjugated to a carboxamide side chain (raltegravir) and by the 4-quinolone-3-carboxylic group (elvitegravir). Looking at these bioisosteric scaffolds, we were interested to determine if they are able to form complexes with two metal ions as DKAs or if they preferentially form coordination compounds with other stoichiometries. The answer is obviously important to clarify the metal chelating mechanism and the activity of these potent IN inhibitors.

Quinolones have been widely used as antibiotics because they are able to selectively inhibit the bacterial DNA gyrase.[36−38] Their interaction with metals was investigated by crystallographic and spectroscopic methods[39−43] as well as by computational tools,[44,45] and their biological activities were extensively explored.[39,46−50] They can form different metal−quinolone complexes, depending on metal to ligand ratio, coordination mode, or the pH conditions. However, most of the complexes present a 1:2 metal to ligand ratio, where the ligand chelates the metal ion through the carboxylate and the ring carbonyl oxygen atoms,[36−38,49−51] whereas only few examples of 1:1 species are available in the literature.[52−54]

Little is known about the coordination behavior of the HPCA backbone.[55] In particular, studies on the biological activity of isolated metal complexes of both classes of inhibitors are surprisingly scarce.

Therefore, to determine which type of metal complexes are formed in solution and what structural features are important for activity, we synthesized a model of the quinolone drug elvitegravir (HL^1, 6-benyl-4-oxo-1,4-dihydroquinolin-3-carboxylic acid) and of raltegravir (HL^2, *N*-(4-fluorobenzyl)-5-hydroxy-1-methyl-2-(1-methyl-1-{[(5-methyl-1,3,4-oxadiazol-2-yl)carbonyl]amino}ethyl)-6-oxo-1,6-dihydropyrimidine-4-carboxamide) (Chart 2). These simplified models are easy to prepare and yet maintain the pharmacophoric backbone of the known inhibitors. In particular, we wanted to elucidate the role of the different pharmachophoric groups in the interaction with the metal ion.

Herein, we report on the synthesis and characterization of HL^1, HL^2, and a series of their metal complexes. The crystal structures of HL^1, HL^2, $[MnL^1_2\cdot 2H_2O]\cdot 2DMSO$, $[MgL^2_2\cdot 2H_2O]$, and $[CoL^2_2\cdot 2H_2O]$ are discussed, together with a potentiometric investigation on the solution behavior of HL^2. Finally, the anti-HIV-1 IN activities of the free ligands and

dx.doi.org/10.1021/jm200851g | J. Med. Chem. 2011, 54, 8407−8420

Chart 2. Chemical Structures of the Model Ligands HL^1 and HL^2

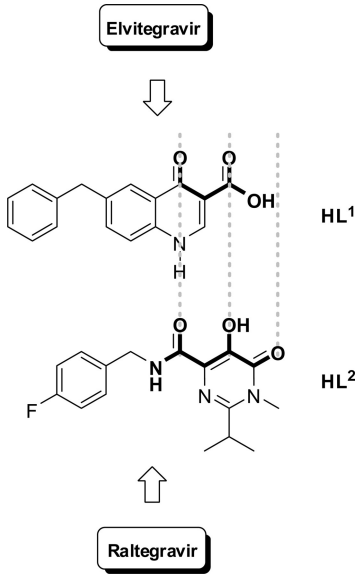

of the metal complexes were evaluated in enzymatic assays, and implications between their structural features and the complexing abilities, as well as a mechanistic hypothesis, are detailed.

RESULTS AND DISCUSSION

Chemistry. Ligands HL^1 and HL^2 were obtained as outlined in Schemes 1 and 2, respectively, according to slightly modified literature procedures.[23,27] HL^1 was obtained from the ester **2** by hydrolysis with 2% NaOH (Scheme 1). **2** was prepared by heating the 4-benzylaniline with diethyl ethoxymethylenemalonate at 130 °C and subsequent thermal cyclization of the aminoacrylate **1** in Dowtherm A for 3 h at reflux conditions (40% yield, method A). Direct condensation and ring closure in Dowtherm A for 5 h provided **2** in modest yield (~27%, method B).

HL^2 was prepared by reaction of the ester **7** with the 4-fluorobenzylamine as described in Scheme 2. The synthesis of the methyl 5,6-dihydroxypyrimidine-4-carboxylate core was achieved by conversion of isobutyronitrile into the amidoxime **3**, followed by reaction with dimethyl acetylenedicarboxylate, to give **4** in quantitative yield. Subsequent cyclization with xylene at reflux afforded the desired intermediate **5**. Finally, **7** was prepared from **5** via regioselective benzoylation of the 5-hydroxyl to provide the intermediate **6**, followed by base-promoted N-methylation in position 1 of the pyrimidone ring. Both ligands were fully characterized by the usual spectroscopic tools and by X-ray diffraction analysis, and the acidic constant of HL^2 was evaluated by potentiometric measurements (see below).

Complexes **8** and **9** were synthesized by reacting the deprotonated ligand HL^1 with $Mg(OH)_2$ and $Mn(CH_3COO)_2$, respectively, in a 2:1 ligand to metal ratio (Scheme 3). The use of a base is necessary to ensure deprotonation of the carboxylic moiety and subsequent coordination to the metal. In the IR spectra, the absorption of the ν(C═O) at 1712 cm^{-1} of the free quinolone was replaced by two strong characteristic bands at 1597, 1420 cm^{-1} (**8**) and 1584, 1407 cm^{-1} (**9**), attributable to the asymmetric and symmetric ν(O−C−O) vibrations, respectively. The $\Delta[\nu(CO_2)_{asym}-\nu(CO_2)_{sym}]$ of 177 cm^{-1} is indicative of a monodentate coordination mode of the carboxylate moiety.[56,57] The pyridone stretching vibration is shifted upon coordination from 1618 to 1560 cm^{-1} (**8**) and 1569 cm^{-1} (**9**). The changes in the IR spectra suggest that the ligand coordinates to the metal through the pyridone and one of carboxylate oxygens.[36−40] ^{1}H NMR, mass spectra, and elemental analysis confirmed the expected stoichiometry, as well as the X-ray diffraction analysis on the manganese complex (see X-ray analysis section). With the aim to prepare 2:2 metal to ligand species,[52] the conditions of the reactions were varied by changing pH, metal/ligand ratio, and metal salt. However, only the monometallic 1:2 metal to ligand species (**8** and **9**) were isolated with no significant amount of 2:2 metal to ligand complexes. For similar reactions, the use of hydrothermal conditions was previously reported[39,52−54] to yield only the 1:2 species.

Complexes **10**−**13** were obtained by reacting HL^2 with the acetate salt of the metal in the presence of NaOH. In this case the use of a base was strictly necessary to deprotonate the ligand, since the pK_a of the hydroxyl moiety was high (see potentiometric section). HL^2 has different coordinating groups that can be involved in coordination, giving rise to five- or six-membered chelating rings (Scheme 3, inset). Therefore, bimetallic species could be present or only one metal could be coordinated, and in this case a 1:2 metal to ligand complex is expected. For compounds **10**−**13**, coordination to the metal ions can be inferred by spectroscopic analysis. In the ^{1}H NMR spectra of both the magnesium and the zinc complexes a downfield shift of the signals of about 0.2 ppm was observed and the resonance of the OH proton, detectable in the free

Scheme 1. Preparation of Ligand HL^1 [a]

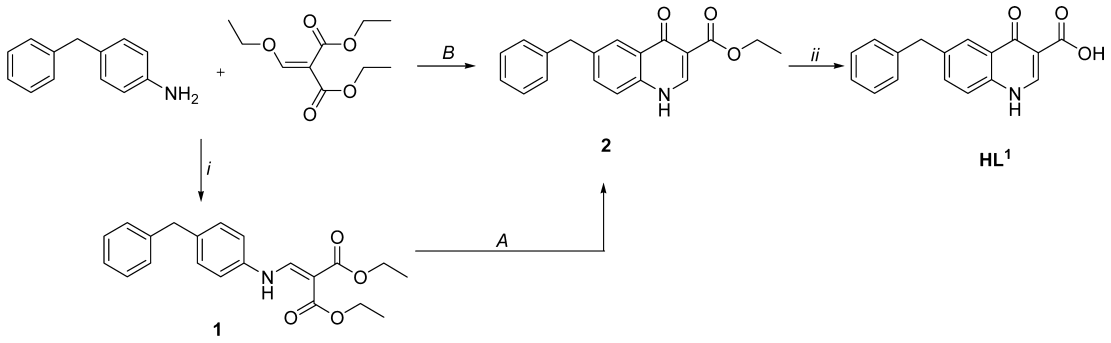

[a]Reagents and conditions: (i) 130 °C for 3 h; (A) Dowtherm A, reflux for 3 h; (B) Dowtherm A, reflux for 5 h; (ii) 2% NaOH, reflux for 3 h.

dx.doi.org/10.1021/jm200851g | J. Med. Chem. 2011, 54, 8407−8420

Scheme 2. Preparation of Ligand HL^2 [a]

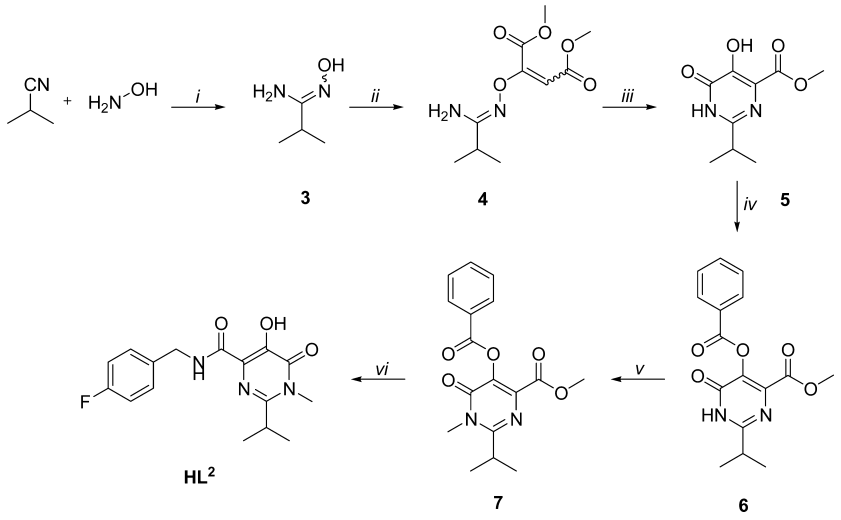

[a]Reagents and conditions: (i) KOH, CH_3OH, room temp, 30 min, then reflux for 24 h; (ii) DMAD, anhyd $CHCl_3$, reflux 24 h; (iii) *o*-xylene, reflux for 48 h; (iv) benzoic anhydride, pyridine, room temp for 48 h; (v) Cs_2CO_3, MeI, anhyd THF, room temp for 24 h; (vi) 4-fluorobenzylamine, anhyd CH_3OH, sealed tube, 70 °C for 3.5 h, then 1 M NaOH, room temp for 30 min.

Scheme 3. Synthesis and Structural Representation of Complexes 8 and 9 (a) and 10–13 (b)

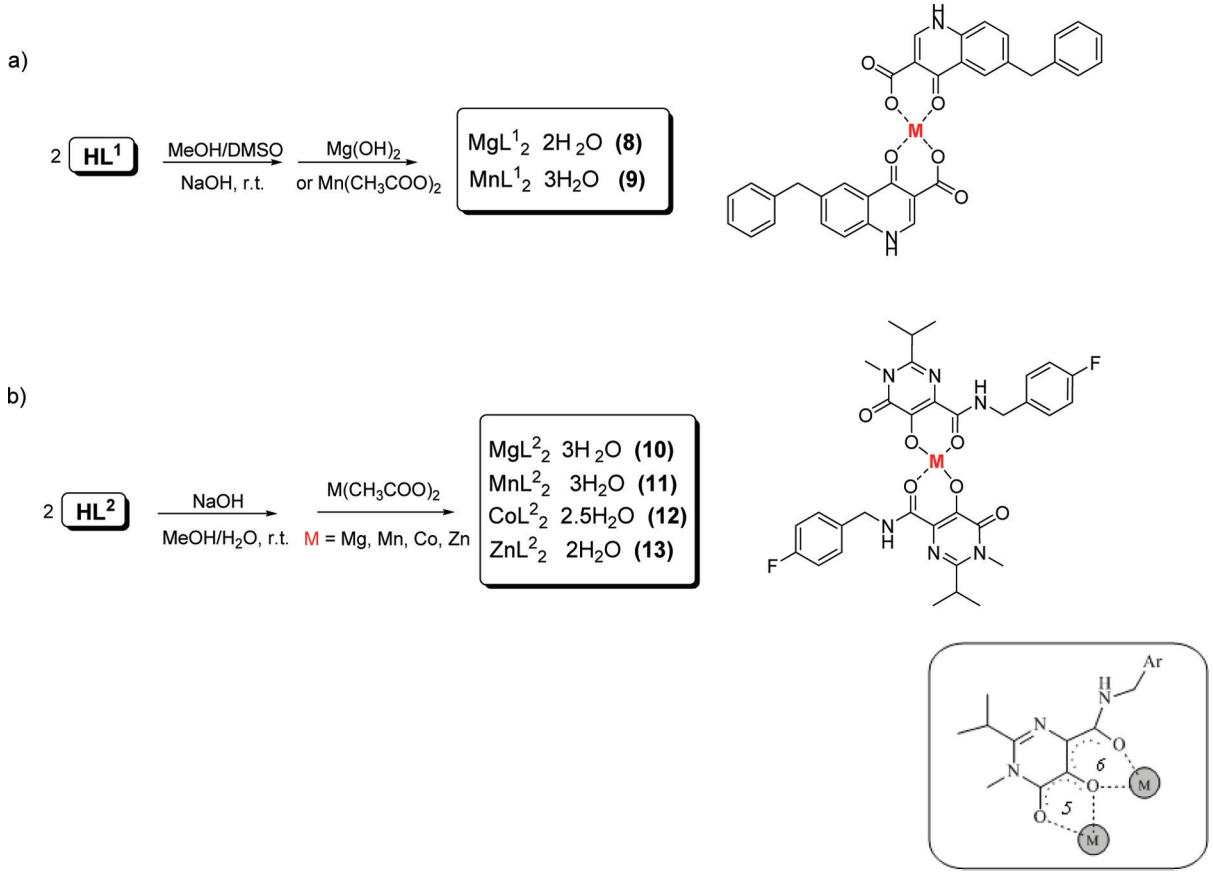

ligand, disappeared. A comparison of the ^{13}C NMR spectra of HL^2 and of **10** suggests that only two of the three coordinating groups (the hydroxyl, the secondary, and the tertiary amides) are involved in the complexation of the metal ion. In fact, with the exception of the one bounded to the isopropyl group, all the resonances of the quaternary carbons were broadened upon coordination, but only the signals attributable to the heterocyclic carbon bonded to the hydroxyl moiety and the carbonyl of the secondary amide are shifted from 168.4 and 157.9 to 166.9 and 165.4 ppm, respectively, indicating the formation of the six-membered ring. In the IR spectra of the complexes, it is possible to observe the shift of the carbonylic stretching absorptions to lower wavenumbers, as well as the upper shift of the NH stretching mode of about 20–40 cm^{-1} vs

dx.doi.org/10.1021/jm200851g | J. Med. Chem. 2011, 54, 8407–8420

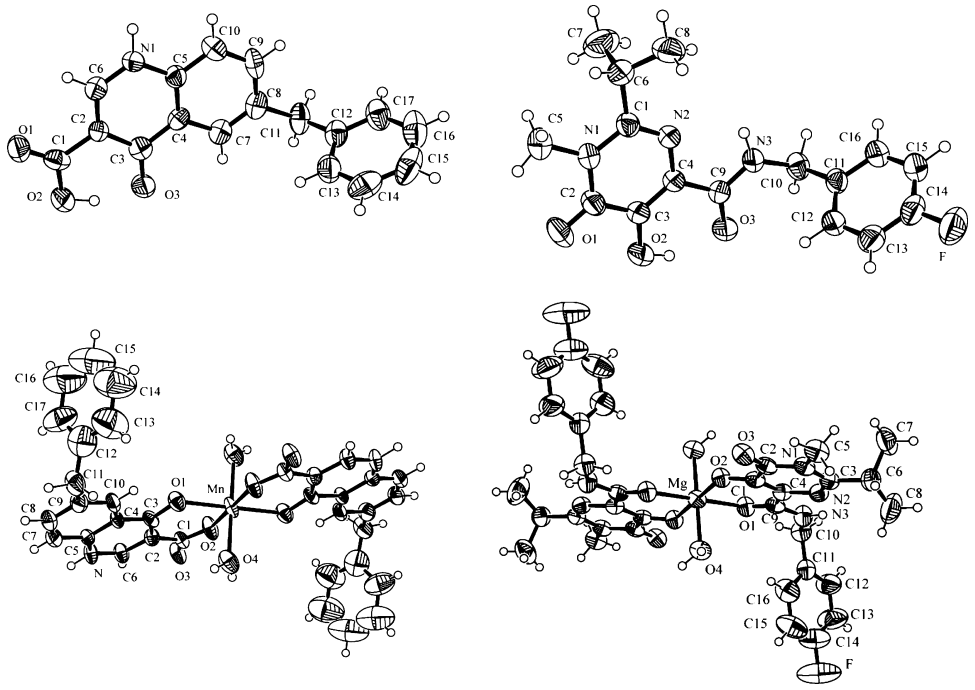

Figure 1. Molecular structures of HL^1 (top left) and HL^2 (top right) and of their complexes with manganese and magnesium, **9** (bottom left) and **10** (bottom right). Thermal ellipsoids are at the 50% probability level.

the free ligand. This is in accord with the involvement of the secondary amide in coordination because the NH group that forms in an intramolecular hydrogen bond in the free ligand is not engaged in any type of interaction after coordination (see X-ray analysis section). In order to exclude the formation of 1:1 species, also with HL^2 several attempts were realized by varying the reaction conditions. All the data (^{1}H NMR, ^{13}C NMR, IR, mass spectrometry, and elemental analysis) confirmed the isolation of the mononuclear, bis-chelated species **10**–**13**. These findings were further supported by potentiometric measurements and calculations.

X-ray Crystallography Studies. To elucidate the pharmacophoric features of the ligands and the coordination geometries of the complexes, a series of X-ray crystallographic studies were carried out. A Mogul[58] analysis of the structure of the two ligands shows that their bonding geometries do not present any unusual feature. HL^1 crystallizes with two independent molecules in the asymmetric unit (only one is shown in Figure 1) that differ only in the conformation of the benzyl substituent around the bond C8–C11 (C9–C8–C11–C12 = 75°, C26–C25–C28–C29 = −111°). Both molecules form an intramolecular hydrogen bond between the carboxylic acid and the quinolone oxygen (O2···O3 = 2.475(6) Å, O–H···O = 159(6)°, O5···O6 = 2.466(6) Å, O–H···O = 144(6)°), while the intermolecular hydrogen bonds between the –NH group and the carboxylic C=O acceptor link the two independent molecules in homomeric chains (N1···O1($-x,y-{}^1/_2,{}^5/_2-z$) = 2.798(7) Å, N–H···O = 177(6)°; N2···O4($-x-1,y-{}^1/_2,{}^5/_2-z$) = 2.853(7) Å, N–H···O = 177(6)°) (see Supporting Information). Similarly, HL^2 presents an intramolecular hydrogen bond between the –OH group and the amidic oxygen (O2···O3 = 2.604(3) Å, O–H···O = 144(3)°), while neighboring molecules are linked in chains by intermolecular hydrogen bonds between the –NH donor and the –OH acting as an acceptor (N3···O2($x,y+{}^1/_2,{}^1/_2-z$) = 3.036(3) Å, N–H···O = 125(2)°) (see Supporting Information). The quinolone oxygen is only involved in weak CH···O contacts.

The crystal structures of **9**, **10**, and **12** are constituted by six-coordinated metal centers binding two bis-chelated deprotonated ligands in the equatorial plane and two water molecules at the apexes of a distorted octahedron (Figure 1; complexes **10** and **12** are isostructural, and only **10** is shown). Compound **9** was obtained from a DMSO solution and crystallized as **9**·2DMSO. All the complexes are centrosymmetric. In the isostructural complexes **10** and **12**, the coordination geometry consists of two six-membered chelation rings that are practically planar, with M–O distances varying between 1.988(5) and 2.080(6) Å and two apical waters at longer distances (2.136(3) Å for Mg and 2.197(6) Å for Co). The rest of the ligand molecules are perfectly coplanar with the equatorial coordination plane, apart form the *p*-fluorobenzyl substituents that stick perpendicularly out of this plane at opposite sides. The crystal packing is described in the Supporting Information.

The coordination geometry in **9** is similar to the one observed for **10** and **12**, with four shorter M–O bonds in the equatorial plane (2.084(7), 2.120(8)Å) and two longer apical metal···water bonds (2.246(8) Å). The difference between corresponding M–O bond lengths in **9**, **10**, and **12** reflects the larger ionic radius of high-spin six-coordinated Mn(II) (0.97 Å) relative to those of high-spin six-coordinated Co(II) (0.88 Å) and six-coordinated Mg(II) (0.86 Å). The benzyl substituents stick out of the average equatorial plane at the opposite sides.

Similar to **10** and **12**, in **9** the coordination consists of two six-membered chelation rings that in this case are puckered in an envelope conformation with the metal at the flap deviating by 0.45 Å from the rest of the ring. Because of the molecular centrosymmetry, the overall effect is that the ligand skeletons are skewed with respect to the apical axis defined by the metal···water coordination bonds. Therefore, the overall molecular shape of **9** is significantly different from **10** and **12** because the ligand planarity is remarkably perturbed. A similar

dx.doi.org/10.1021/jm200851g | J. Med. Chem. 2011, 54, 8407–8420

Table 1. Logarithms of Formation Constants ($\beta_{pqr} = [M_pL_qH_r]/\{[M]^p[L]^q[H]^r\}$) in Methanol/Water = 9:1 v/v, I = 0.1 M KCl at 25 °C for HL^2 with Mg(II), Mn(II), Co(II), and Zn(II)[a]

p	q	r	Mg(II)	Mn(II)	Co(II)	Zn(II)
1	1	0	5.11(0.23)	5.93(0.07)	6.91(0.03)	4.87(0.20)
1	2	0	9.08(0.22)	10.18(0.07)	11.67(0.06)	9.29(0.11)
1	0	−2		−19.88(0.13)	−18.91(0.10)	−19.90(0.22)
0	1	1	L + H = LH		8.639(0.002)	

[a]Standard deviations are given in parentheses. Charges are omitted for simplicity.

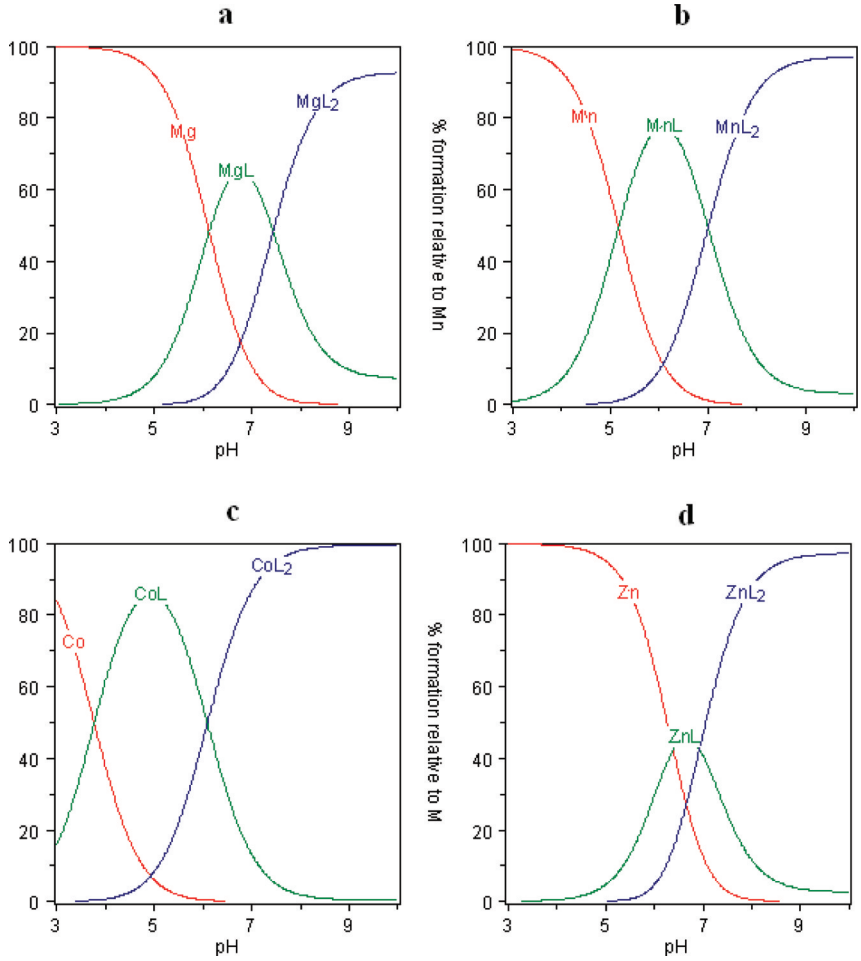

Figure 2. Distribution diagrams for the systems under investigation at L/M = 4:1 (the concentration of the metal ion is 0.75 mM for Mg(II), Mn(II), Co(II) and 0.37 mM for Zn(II)): (a) M = Mg(II); (b) M = Mn(II); (c) M = Co(II); (d) M = Zn(II).

ligand bending is observed in the solvate forms of diaqua-bis(ciprofloxacin)magnesium(II) dinitrate,[42] *rac*-diaqua-bis-(ofloxacin)magnesium(II), and diaqua-bis((*S*)-levofloxacin)-magnesium(II),[41] with the metal displaced by 0.63, 0.56, and 0.43 Å from the chelation plane, respectively. The deformation observed for the ligands skeletons in **9** and in the above cited magnesium complexes may be ascribed to a supramolecular effect, since in **9** the complex crystallizes with one DMSO molecule in the asymmetric unit, which is involved in a extensive network of hydrogen bonds. The steric crowding required for the establishment of this tight network of contacts may consequently force the ligands to bend (Supporting Information, Figure S4). Another interesting observation is that molecular volume and van der Waals surface area of **9** (volume = 494 Å^3, area = 569 Å^2) are significantly smaller than those of **10** and **12** (volume = 548 and 551 Å^3, area = 659 and 654 Å^2).

Potentiometric Measurements and Calculations. A potentiometric study was carried out with Mg^{2+}, Mn^{2+}, Co^{2+}, Zn^{2+}, and HL^2 in order to obtain more information about the type and the stability of the species present at physiological pH. Unfortunately, the poor solubility of HL^1 prevented the same study on the QCA system. The titrations were performed in methanol/water = 9/1 v/v to reduce solubility problems and to obtain results comparable with our previous works.[33,34,59]

HL^2 is a monoprotic acid with a pK_a of 8.639 ± 0.002. A pK_a of 6.48 was reported for a similar ligand based on 6-carboxamido-5,4-hydroxypyrimidinones (6-carboxamido-5,4-HOPY) in aqueous solution at the same ionic strength.[55] The different value we found for HL^2 can be explained by the use of mixed solvents and by the different functionalizations of the two ligands.

The stoichiometry of the complexes with Mg^{2+}, Mn^{2+}, Co^{2+}, and Zn^{2+} were determined by using metal to ligand ratios from

dx.doi.org/10.1021/jm200851g | J. Med. Chem. 2011, 54, 8407–8420

1:1 to 1:5. Titrations with Zn^{2+} must be performed at halved concentrations because of poor solubility. Results of the best fit of the experimental titration curves by the Hyperquad software[60] are reported in Table 1, and the corresponding distribution diagrams are shown in Figure 2 for a metal/ligand ratio of 1/4.

The species found in solution were $[ML]^+$ and ML_2 for all the studied metal ions, with formation constants that increase in the order $Zn^{2+} < Mg^{2+} < Mn^{2+} < Co^{2+}$ for the ML complex and in the order $Mg^{2+} \sim Zn^{2+} < Mn^{2+} < Co^{2+}$ for the ML_2 complex, according to the Irving–Williams sequence.[61]

This model is statistically significant, and we observe a reasonable correlation between experimental and computed titration curves. For Co^{2+} and Zn^{2+}, convergence can be achieved only by considering the hydrolysis of the cation, by adding the formation constant of the hydroxide (Table 1). Interestingly, at physiological conditions, both species (ML and ML_2) are present, and Co(II) is the only ion almost completely in the form of the ML_2 complex (Figure 2).

Therefore, HL^2 behaves in a different way with respect to DKA ligands:[33,34] whereas at physiologic pH the parent DKAs are almost completely in the form M_2L_2 with a metal/ligand = 1/1, this ratio is less favored with HL^2 (in particular the species M_2L_2 cannot be found in solution) and the formation constants of ML_2 complexes are much greater than for the other species in solution.

Inhibition of HIV-1 IN. The ligands HL^1 and HL^2 and their complexes **8**–**13** were tested for their ability to inhibit 3′-processing and strand transfer catalytic activities by employing purified enzyme (Table 2). Both series of compounds showed inhibition potency in the low nanomolar/micromolar concentration range, with significant selectivity toward strand transfer.

Table 2. Inhibition of HIV-1 IN Catalytic Activities of Ligands and Complexes

		IC_{50} (μM)		
compd	M[a]	3′-processing	strand transfer	SI[b]
HL^1		>100	12 ± 5	>8.3
8	Mg^{2+}	89 ± 16	4 ± 2	22.2
9	Mn^{2+}	>250	2 ± 0.1	>125
HL^2		10 ± 8	0.14 ± 0.03	71.4
10	Mg^{2+}	8 ± 5	0.41 ± 0.2	19.5
11	Mn^{2+}	7 ± 4	0.18 ± 0.1	38.9
12	Co^{2+}	1.9 ± 1.1	0.09 ± 0.02	21.1
13	Zn^{2+}	2.6 ± 1.0	0.23 ± 0.10	11.3

[a]M, metal ion. [b]SI, selectivity index.

In particular, HL^2 (IC_{50}, strand transfer = 0.14 ± 0.03 μM; 3′-processing = 10 ± 8 μM) was about 100-fold more potent than the quinolone HL^1 (IC_{50}, strand transfer = 12 ± 5 μM; 3′-processing > 100 μM). The complexes **8**–**13** retained an activity profile analogous to the corresponding free ligands, as already observed in our previous work on DKAs and triazolic bioisosters[33,34,59] (Table 2; for a representative gel, see Figure 3).

The magnesium and manganese complexes of **8** and **9** resulted in a 4-fold and 6-fold increase in activities with respect to the parent ligand (IC_{50}, strand transfer of 4 ± 2 and 2 ± 0.1 μM for **8** and **9**, respectively, vs 12 ± 5 μM for HL^1), and **9** was 2-fold more potent than **8** (Figure 3b). Interestingly, when HL^1 was involved in coordination, an enhancement in potency was observed, thus demonstrating that both the metals and organic scaffold are important for the activity.

Different behavior was found for compounds bearing the HMPCA-based pharmacophoric motif. In fact, the strand transfer inhibition values for complexes **10**–**13** ranged from 0.09 to 0.41 μM, thus sharing a potency similar to that of the free ligand HL^2 (Figure 3). As already observed in our previous study on triazole derivatives,[59] the Co(II) complex **12** proved to be the most active tested compound, with an IC_{50} value of 0.09 ± 0.02 for strand transfer. Therefore, an interesting metal-dependent behavior was evidenced also for HL^2 and its metal complexes. The activity of the complexes toward strand transfer, even if with slight differences, follows the trend Mg < Zn < Mn < Co [IC_{50}, strand transfer = 0.41 ± 0.2, 0.23 ± 0.10, 0.18 ± 0.1, 0.09 ± 0.02 μM for Mg(II), Zn(II), Mn(II), Co(II), respectively].

The activity of the metal complexes enforced the observation that they are quite stable in solution (see also their log β values) and that the complexes, not necessarily only the free ligand, might be involved in the inhibition mechanism (Figure 4). Another point that would support this hypothesis regards the Co(II) complex. The reaction buffer for the assay contains Mn^{2+} in millimolar concentration, to ensure enzymatic activity, and other ligands (EDTA, DTT). When the metal complex is dissolved, equilibria between the different metal species in solution arise, according to the different formation constants and concentrations. Interestingly, the Co(II) complex, which has the higher stability constant, also shows the higher anti-IN activity.

Monometallic Species in Strand Transfer Inhibition. The analysis of the coordinating ability of both the HPCA and the QCA pharmachophoric models indicates that in solution the formation of monometallic species is more plausible than the concurrent chelation of two metal centers. On the other hand, the possibility of formation, in proximity of the chelation region, of other types of interactions like hydrogen bonds would also exert a crucial role for binding into the active site (for example, by mediating the interaction with the protein side chain). Effectively, a tight network of supramolecular hydrogen bonds is observed in the crystal packing of the complexes, involving the noncoordinated carboxylic oxygen (complex **9**) or the pyrimidone oxygen (**10**).

At this stage, it can be proposed that in the presence of metal ions, the HMPCA- and QCA-based chemical pharmacophores form complexes that could bind directly to IN, after keeping and/or scavenging the metal, interacting as single static entity (Figure 4). ML and ML_2 could also bind to IN and engage the second ion cofactor that is present on the active site. Either way, the values of the stability constants of the complexes, the concentration of divalent cation in the assays conditions, and the similar inhibition data for the free ligand and the corresponding complexes support the hypothesis of the complexes as putative active forms of the IN inhibitors, indicating that stable species present in solution are involved in several ways in the inhibitory action. This concept was also suggested in our previous studies.[33,34,59]

An "interfacial-type mechanism" of action for metal complexes, where the chelation of the Mg^{2+} ion in the active site of IN is important for the activity of the inhibitor, is also possible. The inhibitors could interact with IN after 3′-processing or in the later stage of this process. After binding to the enzyme as preformed complexes, a DNA-induced conformational change occurs, displacing the reactive viral

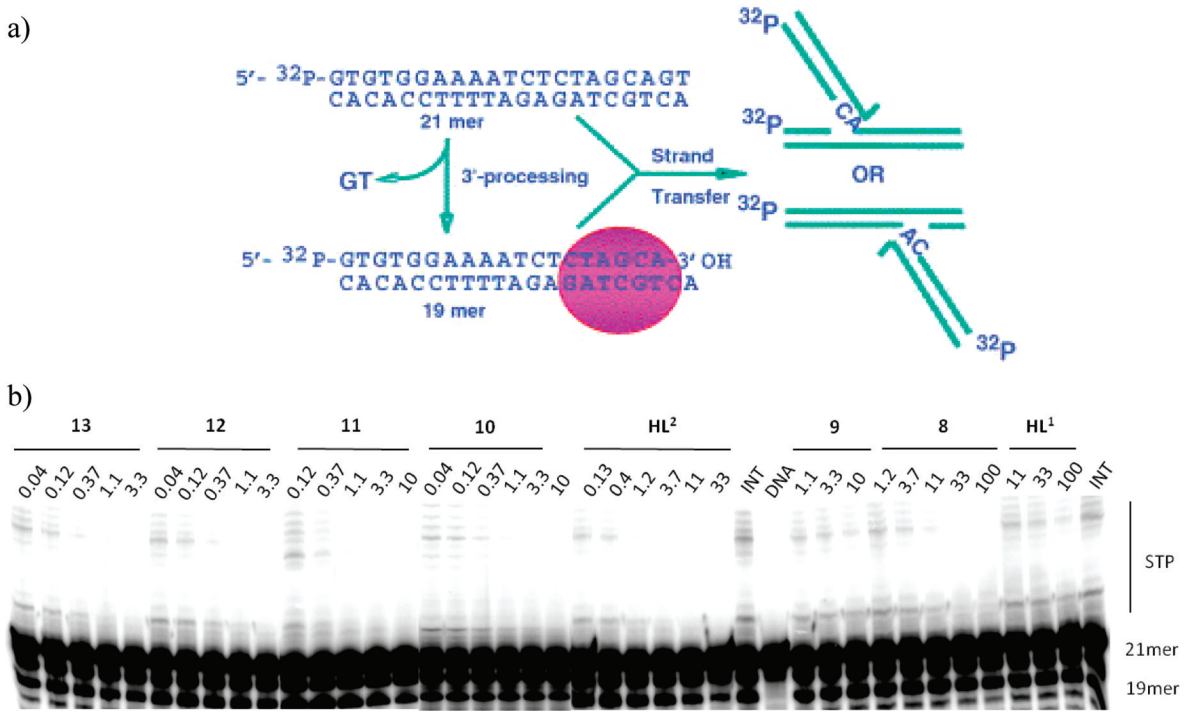

Figure 3. Schematic representation of IN activity in vitro and representative gel showing inhibition of purified IN by HL[1], HL[2], and **8**−**13**. (a) A 21-mer blunt-end oligonucleotide corresponding to the U5 end of the HIV-1 LTR, 5′ end-labeled with ^{32}P, is reacted with purified IN. The first step (3′-P) involves nucleolytic cleavage of two bases from the 3′ end, resulting in a 19-mer oligonucleotide. Subsequently, 3′ ends are covalently joined at several sites to another identical oligonucleotide that serves as the target DNA (ST). The products formed by this reaction migrate more slowly than the original substrate on a polyacrylamide gel. (b) Line labeled as DNA indicates DNA alone. Line labeled INT indicates IN and DNA with no drug. Other lines are as follows: IN, DNA, and selected drug concentrations (μM) as indicated in each line.

DNA end from the active site and thus disarming the viral nucleoprotein complex. It is also possible to speculate that inhibitors bind to a transient IN-DNA structure formed prior to or upon 3′-OH processing within the cytosolic preintegration complex. This can explain why, among the identified IN inhibitors that specifically target the strand transfer reaction alone, several of them are highly selective for strand transfer while others also show some activity against the 3′-processing reaction. Therefore, the reactive species could be the metal complex that specifically interacts with the protein and prevents the interaction between the enzyme and its DNA (viral) substrate.

Recently, a crystal structure of the quinolonic drug moxifloxacin in complex with *Acinetobacter baumannii* topoisomerase IV revealed that a magnesium ion mediates the interaction between the drug and the protein, suggesting that an "interfacial model" could also be at the base of the mode of action of quinolone antibacterial drugs.[62]

CONCLUSIONS

The studies on HIV-1 IN inhibitors and on the biology of metal cofactors have confirmed the important role of the metals in the inhibition process and consequently that the metal binding function is a critical factor in the development of IN inhibitors. The compounds related to the diketo acids family, such as raltegravir and elvitegravir, are well suited to explore this chemical space, and they represent milestones for medicinal chemistry discovery and development programs. These molecules contain the basic structural features that established what is known as the "two-metal chelation" motif. Effectively, we have confirmed that these inhibitors can chelate metal ions, giving stable, isolable species. We have also observed that the complexes themselves inhibit the HIV-1 IN catalytic activities and, moreover, that their activity is metal dependent. This means that the metal complexes (in particular the Mg(II) complex at physiological conditions) could be involved in different stages of the inhibition process. Another relevant point is that the complexes that we have characterized are monometallic and as such can participate in the inhibition mechanism by interacting with the enzyme in many ways (i.e., exchange of the metals, coordination of a second metal, second coordination sphere interactions). Molecular modeling studies that consider this hypothesis are in progress in our laboratory. We anticipate that the results presented here can contribute to the mechanistic aspect of HIV-IN inhibitors action and can expedite the design of other metal-based complexes for different targets.

EXPERIMENTAL SECTION

Materials and Methods. Chemistry. Anhydrous solvents and all reagents were purchased from Sigma-Aldrich, Merck, or Carlo Erba and used without further purification. All reactions involving air- or moisture-sensitive compounds were performed under a nitrogen atmosphere using oven-dried glassware and syringes to transfer solutions. Purity of compounds was determined by elemental analysis and verified to be ≥95% for all synthesized molecules. Elemental analyses were performed by using a Carlo Erba model EA 1108 apparatus and were within ±0.4% of the theoretical values.

Melting points (mp) were determined using an Electrothermal melting point or a Köfler apparatus and are uncorrected. Analytical thin-layer chromatography (TLC) was carried out on Merck silica gel F-254 plates. Flash chromatography purifications were performed on Merck silica gel 60 (230−400 mesh ASTM) as the stationary phase.

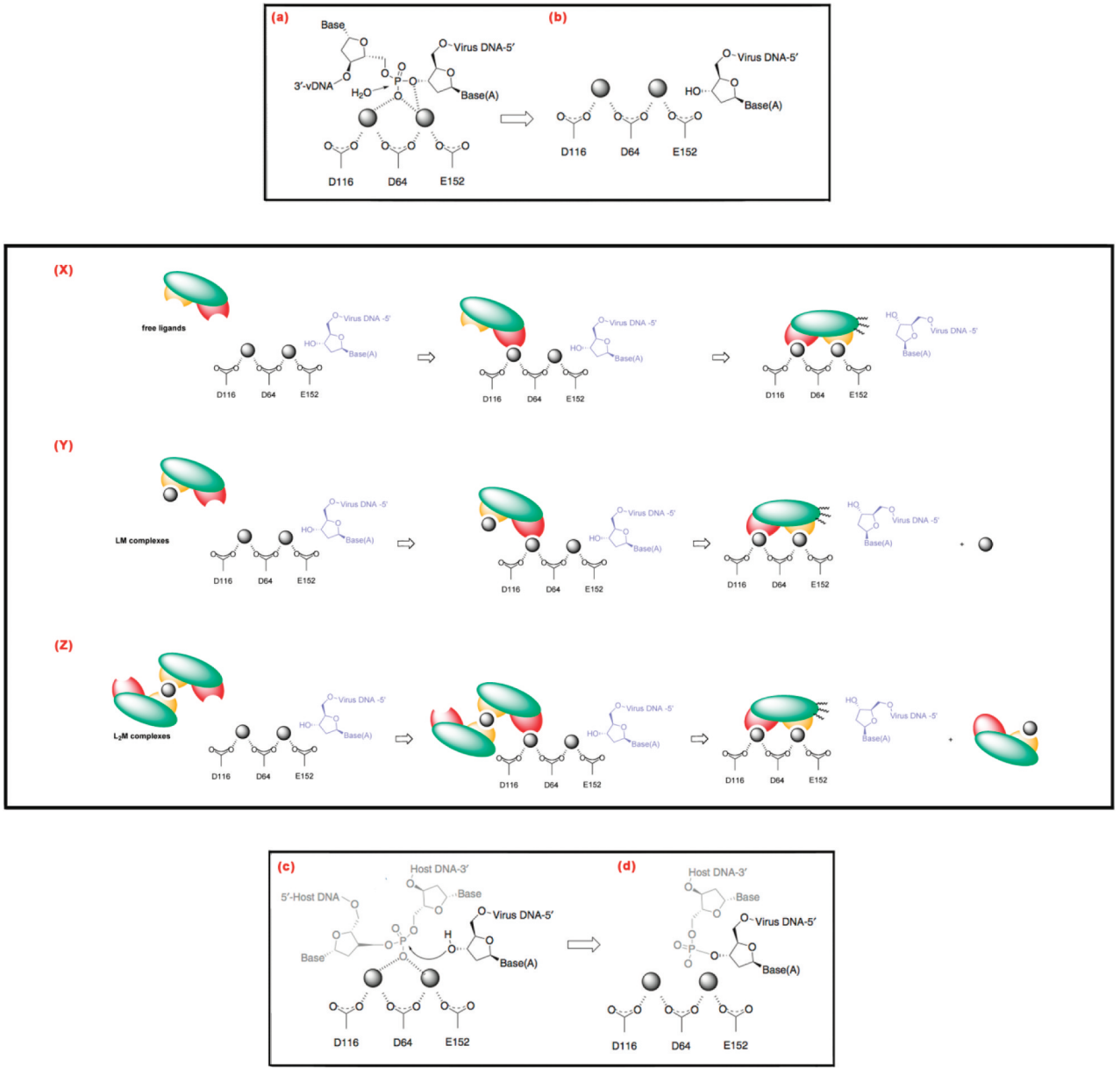

Figure 4. Mechanism of proviral DNA integration and proposed mechanistic model for SSTI and related complexes. The integration process of the HIV lifecycle requires two steps mediated by the IN enzyme, 3′-end processing (a, b) and strand transfer reaction (c, d). Stage **a** to **b**: IN removes the last dinucleotide in 3′ position to the conserved CA of viral DNA, thanks to the catalytic action of the metal cofactors. The recognized adenosine is exposed as the new 3′-end, still bound to the protein as PIC (preintegration complex). From stage c to d, the PIC nonspecifically binds to host DNA and the two metals catalyze a five staggered base pair cut into host DNA, linking both viral 3′ ends and achieving integration of viral DNA into the host genome. In the inhibition mechanism, inhibitors can bind as free ligands (X) or as preformed ML (Y) or ML_2 (Z) complexes to the active site within or after the 3′-processing. Complexes would bind directly to IN, after keeping and/or scavenging the metal, to form a ternary ligand–M^{2+}–IN complex. This would represent the first step of the inhibition process. Next, after accommodation within the active site, ligands or complexes can interact with a second ion by interfering with the viral DNA substrate. In this manner the inhibitors cause a displacement of the reactive viral DNA end from the active site, blocking DNA binding.

NMR spectra were recorded at 27 °C on Bruker Avance 300 FT and Varian XL-200 spectrophotometers by using $SiMe_4$ as internal standard; the assignment of exchangeable protons (O*H* and N*H*) was confirmed by the addition of D_2O. IR spectra were obtained with a Nicolet 5PCFT-IR spectrophotometer in the 4000–400 cm^{-1} range, in reflectance mode on the powder. The ESI(+)-MS spectra were collected by using a quadrupole-time-of-flight Micromass spectrometer (Micromass, Manchester, U.K.) equipped with a pneumatically assisted ESI interface. The system was controlled by Masslynx software, version 4.0 (Micromass). The nebulizing gas (nitrogen, 99.999% purity) and the desolvation gas (nitrogen, 99.998% purity) were delivered at a flow rate of 10 and 600 L/h, respectively. Continuum mode full-scan mass spectra were acquired using an acquisition time of 1 s and an interscan delay of 0.1 s. QqTOF external calibration was performed using a 0.1% phosphoric acid solution, and a fifth-order nonlinear calibration curve was usually adopted.

Synthesis of Ethyl 2-((4-Benzylphenylamino)methylen)-malonate (1). A mixture of 4-benzylaniline (5 g, 27.3 mmol) and diethyl ethoxymethylenemalonate (5.9 g, 27.3 mmol) was stirred at 130 °C for 3 h. On elimination of the volatile components, a brown oil was obtained, which was used without further purification. Quantitative yield. IR (Nujol, cm^{-1}): $\nu_{C=O}$ = 1752, 1645. ^1H NMR ($CDCl_3$): δ 11.01 (d, 1H, J = 14 Hz, NH); 8.50 (d, 1H, J = 14 Hz, CH); 7.34–7.17 (m, 5H, Ar-H); 7.06 (d, 2H, Ar-H, $^3J_{HH}$ = 8 Hz); 4.30

dx.doi.org/10.1021/jm200851g | J. Med. Chem. 2011, 54, 8407–8420

(q, 2H, OCH_2, $^3J_{HH}$ = 6.2 Hz); 4.27 (q, 2H, OCH_2, $^3J_{HH}$ = 6.5 Hz); 3.97 (s, 2H, CH_2); 1.38 (t, 3H, CH_3, $^3J_{HH}$ = 6.3 Hz); 1.32 (t, 3H, CH_3, $^3J_{HH}$ = 6.6 Hz).

Synthesis of Ethyl 6-Benzyl-4-oxo-1,4-dihydroquinolin-3-carboxylate (2). *Method A.* A solution of **1** (9.6 g, 27.3 mmol) in Dowterm A (30 mL) was stirred at reflux for 3 h and then cooled at room temperature. By addition of petroleum ether, a beige powder was obtained, which was filtered off and washed several times with petroleum ether. Yield: 40%.

Method B. 4-Benzylaniline and diethyl ethoxymethylenemalonate in equimolar amount were stirred at 130 °C for 5 h. Workup was analogous to method A. Yield: 27%.

IR (cm^{-1}): $\nu_{C=O}$ = 1744, 1631. ^1H NMR (DMSO-d_6): δ 12.33 (s, br, 1H, NH); 8.51 (s, 1H, CH); 7.97 (s, 1H, Ar-H); 7.56 (m, 2H, Ar-H); 7.30−7.19 (m, 5H, Ar-H); 4.23 (q, 2H, OCH_2, $^3J_{HH}$ = 6.4 Hz); 4.07 (s, 2H, CH_2); 1.27 (t, 3H, CH_3, $^3J_{HH}$ = 6.6 Hz). ESI/MS (+, *m*/*z*): 307 [MH^+].

Synthesis of 6-Benyl-4-oxo-1,4-dihydroquinolin-3-carboxylic Acid (HL^1). A solution of **2** (3.35 g, 10.9 mmol) and 2% NaOH (11 mL) was refluxed for 3 h and then acidified at room temperature by using 1 N HCl. The precipitate was filtered off and recrystallized from water/ethanol, giving rise to a white powder. Yield: 97%. Mp: 234−235 °C (dec). IR (cm^{-1}): $\nu_{C=O}$ = 1687, 1618. ^1H NMR (DMSO-d_6): δ 15.41 (s, br, OH); 13.43 (s, br, 1H, NH); 8.85 (s, 1H, CH); 8.23 (s, 1H, Ar-H); 8.00 (d, 1H, Ar-H, $^3J_{HH}$ = 9 Hz); 7.81 (d, 1H, Ar-H, $^3J_{HH}$ = 8.1 Hz); 7.27 (m, 5H, Ar-H); 4.14 (s, 2H, CH_2). ^{13}C NMR (DMSO-d_6): δ 178.2, 166.6, 144.8, 140.6, 139.9, 138.1, 135.1, 128.9, 128.7, 126.3, 124.5, 124.1, 120.0, 107.5, 40.6. ESI/MS (+, *m*/*z*): 279 [MH^+]. Crystallization from chloroform afforded crystals suitable for X-ray diffraction analysis.

Synthesis of *N*′-Hydroxy-2-methylpropanimideamide (3). Hydroxylamine chlorohydride (3 g, 43 mmol) was dissolved in 30 mL of methanol, and to the mixture was added KOH (2.7 g, 48 mmol). After the mixture was stirred for 30 min, KCl was filtered off and washed several times with methanol. Isobutyronitrile (3 g, 43 mmol) was added and the reaction mixture refluxed for 24 h. On elimination of the solvent, a yellow oil was obtained. Yield: 85%. ^1H NMR ($CDCl_3$): δ 8.08 (s, br, OH); 4.58 (s, br, 2H, NH_2); 2.45 (m, 1H, CH, $^3J_{HH}$ = 6.9 Hz); 1.19 (dd, 6H, CH_3, $^3J_{HH}$ = 6 Hz). ESI/MS (+, *m*/*z*): 102 [M^+].

Synthesis of Dimethyl 2-(1-Amino-2-methylpropylidenaminooxy)but-2-endioate (4). An amount of 3.7 g (36 mmol) of **3** was dissolved in 20 mL of distilled $CHCl_3$ under anhydrous conditions. To the mixture was added dropwise a 15 mL solution of dimethylacetylene dicarboxylate (6.3 g, 44.6 mmol). The reaction mixture turned yellow. It was refluxed for 24 h and then dried under vacuum. A brown oil was obtained. Quantitative yield. ^1H NMR ($CDCl_3$) major isomer: δ 5.87 (s, 1H, =CH); 4.74 (s, br, 2H, NH_2); 3.97 (s, 3H, CH_3); 3.72 (s, 3H, CH_3); 2.50 (overlapping signals, CH); 1.20 (overlapping signals, CH_3). Minor isomer: δ 5.76 (s, 1H, =CH); 5.52 (s, br, 1H, NH); 5.22 (s, br, 1H, NH); 3.84 (s, 3H, CH_3); 3.74 (s, 3H, CH_3).

Synthesis of Methyl 5-Hydroxy-2-isopropyl-6-oxo-1,6-dihydroxypyrimidine-4-carboxylate (5). An amount of 36 mmol of **4** (8.8 g) was dissolved in 115 mL of *o*-xylene, obtaining a brown solution that was refluxed for 48 h. The reaction was monitored by TLC (CH_2Cl_2/MeOH, 3%). On evaporation of the solvent, a dark oil was obtained. It was dissolved in warm ethyl acetate. When the mixture was cooled at −18 °C, a brown solid precipitated, which was further recrystallized from ethyl acetate. Yield: 30%. IR (cm^{-1}): ν_{OH} = 3167; $\nu_{C=O}$ = 1704, 1672. ^1H NMR (DMSO-d_6): δ 12.66 (s, br, 1H, OH); 10.17 (s, br, 1H, NH); 3.81 (s, 3H, CH_3); 2.77 (m, 1H, CH, $^3J_{HH}$ = 6.4 Hz); 1.16 (d, 6H, CH_3, $^3J_{HH}$ = 6.7 Hz). ESI/MS (+, *m*/*z*): 212 [M^+].

Synthesis of Methyl 5-Benzyloxy-2-isopropyl-6-oxo-1,6-dihydroxypyrimidine-4-carboxylate (6). An amount of 2.3 g (11 mmol) of **5** and an equimolar amount of benzoic anhydride were suspended in 30 mL of dry pyridine under anhydrous conditions. After 1 h the solution was clear. It was stirred at room temperature for 48 h. The reaction was monitored by TLC (ethyl acetate, 100%). The solution was quenched with 1 N HCl and extracted with 30 mL of ethyl acetate. The organic layer was washed three times with 1 N HCl and twice with brine, then dried with Na_2SO_4. On elimination of the solvent, a white solid was obtained, which was treated with diethyl ether, filtered off, and dried in air. Yield: 85%. IR (cm^{-1}): ν_{NH} = 3172; $\nu_{C=O}$ = 1740, 1681. ^1H NMR (DMSO-d_6): δ 13.29 (s, br, 1H, NH); 8.07 (d, 2H, Ar-H, $^3J_{HH}$ = 7.2 Hz); 7.78 (t, 1H, Ar-H, $^3J_{HH}$ = 7.5 Hz); 7.63 (t, 2H, Ar-H, $^3J_{HH}$ = 7.6 Hz); 3.75 (s, 3H, CH_3); 2.91 (m, 1H, CH, $^3J_{HH}$ = 6.9 Hz); 1.23 (dd, 6H, CH_3 $^3J_{HH}$ = 6.3 Hz). ESI/MS (+, *m*/*z*): 316 [M^+].

Synthesis of Methyl 5-Benzyloxy-2-isopropyl-1-methyl-6-oxo-1,6-dihydroxypyrimidine-4-carboxylate (7). An amount of 3 g (9 mmol) of **6** was dissolved in 100 mL of distilled THF under anhydrous conditions, and to the mixture was added 2 equiv of Cs_2CO_3. After the mixture was stirred for 20 min at room temperature, an amount of 26 mmol (3.7 g) of CH_3I was added dropwise and the reaction mixture was stirred for 24 h. The solution was diluted with 1 N HCl and then extracted with ethyl acetate. The organic layer was washed with brine and then dried with Na_2SO_4. On elimination of the solvent, a brown, hygroscopic solid was obtained, which was used without further purification. Yield: 97%. IR (cm^{-1}): $\nu_{C=O}$ = 1737, 1687. ^1H NMR ($CDCl_3$): δ 8.20 (d, 2H, Ar-H, $^3J_{HH}$ = 7.2 Hz); 7.64 (t, 1H, Ar-H, $^3J_{HH}$ = 7.4 Hz); 7.51 (t, 2H, Ar-H, $^3J_{HH}$ = 7.8 Hz); 3.85 (s, 3H, CH_3); 3.68 (s, 3H, CH_3); 3.17 (m, 1H, CH, $^3J_{HH}$ =6 0.4 Hz); 1.39 (d, 6H, CH_3, $^3J_{HH}$ = 6.8 Hz). ESI/MS (+, *m*/*z*): 330 [M^+].

Synthesis of *N*-(4-Fluorobenzyl)-5-hydroxy-2-isopropyl-1-methyl-6-oxo-1,6-dihydroxypyrimidine-4-carboxylate (HL^2). An amount of 2.9 g (8.7 mmol) of **7** was dissolved in 40 mL of methanol in a sealed tube, and to the mixture was added dropwise 2 equiv (2.2 g) of 4-fluorobenzylamine. The mixture was refluxed for 3 h. After the mixture was cooled at room temperature, an amount of 10 mL of 1 M NaOH was added. The solution was stirred for 30 min at room temperature, then diluted with 20 mL of water and extracted with CH_2Cl_2. The aqueous layer was treated with 1 N HCl. At neutral pH a white precipitate appeared, which was filtered off and washed with water. Yield: 80%. IR (cm^{-1}): ν_{NH} = 3339; $\nu_{C=O}$ = 1673, 1636. ^1H NMR (DMSO-d_6): δ 12.14 (s, br, 1H, OH); 9.21 (s, br, 1H, NH); 7.38 (dd, 2H, Ar-H, $^3J_{HH}$ = 7.0 Hz); 7.17 (dd, 2H, Ar-H, $^3J_{HH}$ = 8.7 Hz); 4.49 (d, 2H, CH_2, $^3J_{HH}$ = 6.3 Hz); 3.52 (s, 3H, CH_3); 3.15 (m, 1H, CH, $^3J_{HH}$ = 6.6 Hz); 1.25 (d, 6H, CH_3, $^3J_{HH}$ = 6.6 Hz). ^{13}C NMR (DMSO-d_6): δ 168.4 (H_d); 160.8 (d, J_{C-F} = 324 Hz); 157.9 (H_b); 155.7 (H_a); 145.5; 134.8; 129.2 (d, J_{C-C} = 10 Hz); 124.9 (H_c); 115.0 (d, J_{C-C} = 28 Hz); 41.4; 30.8; 30.3; 20.4. ESI/MS (+, *m*/*z*): 319 [M^+]. Crystallization from chloroform afforded crystals suitable for X-ray diffraction analysis.

Synthesis of $MgL^1_2 \cdot 2H_2O$ (8). HL^1 (97 mg, 0.35 mmol) was dissolved in 4 mL of methanol and 6 mL of dimethylsulfoxide, and to the mixture was added 1.2 equiv of 0.1 M NaOH. The solution was stirred at room temperature for 30 min, and then $Mg(OH)_2$ (10 mg, 0.17 mmol) was added. The reaction mixture was stirred for 24 h at room temperature. On elimination of the solvent a white powder was isolated, which was washed with water and dried under vacuum. Yield: 78%. IR (cm^{-1}): ν_{NH} = 3356; $\nu_{C=O}$= 1597, 1569, 1420. ^1H NMR (DMSO-d_6): δ 16.66 (s, br, 1H, NH); 8.78 (s, 1H, =CH); 8.03 (s, 1H, Ar-H); 7.67 (br, 2H, Ar-H); 7.28 (m, br, 5H, Ar-H) 4.11 (s, 2H, CH_2). ESI/MS (+, *m*/*z*): 581 [MH^+]; 603 [M + Na^+].

Synthesis of $MnL^1_2 \cdot 3H_2O$ (9). HL^1 (97 mg, 0.35 mmol) was dissolved in 30 mL of methanol and 3 mL of dimethylsulfoxide, and to the mixture was added 1.2 equiv of 0.1 M NaOH. The solution was stirred at room temperature for 30 min, and then an aqueous solution of $Mn(CH_3COO)_2$ (44 mg, 0.17 mmol) was added. Immediately, a yellow precipitate was formed, which was stirred for an additional 4 h. The solution was concentrated on vacuum and the solid filtered off and washed with water. Yield: 82%. IR (cm^{-1}): ν_{NH} = 3446; $\nu_{C=O}$= 1584, 1560, 1407. ESI/MS (+, *m*/*z*): 634 [M + Na^+]. X-ray diffraction quality crystals were obtained by recrystallization from DMSO as $MnL^1_2 \cdot 2DMSO$.

Synthesis of $MgL^2_2 \cdot 3H_2O$ (10). HL^2 (96 mg, 0.3 mmol) was dissolved in 20 mL of methanol, and to the mixture was added 1.2 equiv of 0.1 M NaOH. After the mixture was stirred at room

temperature for 30 min, an aqueous solution of Mg-$(CH_3COO)_2{\cdot}4H_2O$ (0.15 mmol) was slowly added and a white precipitate appeared. The reaction mixture was stirred at room temperature for 3 h, and the precipitate was filtered off and washed with water. Yield: 77%. IR (cm^{-1}): ν_{NH} = 3358; $\nu_{C=O}$= 1660, 1621. ^1H NMR (DMSO-d_6): δ 9.57 (s, br, 1H, NH); 7.21 (s, br, 2H, Ar-H); 6.93 (s, br, 2H, Ar-H); 4.35 (s, 2H, CH_2); 3.44 (s, 3H, NCH_3); 3.05 (m, 1H, CH); 1.18 (t, 6H, CH_3). ^{13}C NMR (DMSO-d_6): δ 166.9 (br, H_d); 165.4 (br, H_b); 160.8 (d, J_{C-F} = 324 Hz); 155.0 (br, H_a); 144.7; 135.8; 129.2 (d, J_{C-C} = 10 Hz); 125.9 (br, H_c); 114.6 (d, J_{C-C} = 28 Hz); 41.0; 30.1; 30.0; 20.8. Recrystallization from methanol/water afforded crystals of $MgL^2_2{\cdot}2H_2O$ suitable for X-ray diffraction analysis.

Synthesis of $MnL^2_2{\cdot}3H_2O$ (11). Compound **11** was prepared using the same protocol as described for **10** using Mn-$(CH_3COO)_2{\cdot}4H_2O$. The solution became immediately bright yellow and was stirred for 3 h at room temperature. On concentration of the solution, a yellow precipitate appeared, which was filtered off and washed with water. Yield: 70%. IR (cm^{-1}): ν_{NH} = 3375; $\nu_{C=O}$= 1616 (br). ESI/MS (+, m/z): 714 [M + Na^+].

Synthesis of $CoL^2_2{\cdot}2.5H_2O$ (12). Compound **12** was prepared using the same protocol as described for **10** using Co-$(CH_3COO)_2{\cdot}4H_2O$. The solution turned light red, and the reaction mixture was stirred at room temperature for 3 h. The solvent was eliminated on vacuum, and the residue was suspended in diethyl ether, filtered off, and washed with water. A red powder was obtained. Yield: 74%. IR (cm^{-1}): ν_{NH} = 3375; $\nu_{C=O}$= 1621 (br). Recrystallization from methanol/water, 5/1, afforded crystals of $CoL^2_2{\cdot}2H_2O$ suitable for X-ray diffraction analysis.

Synthesis of $ZnL^2_2{\cdot}2H_2O$ (13). Compound **13** was prepared using the same protocol as described for **10** using Zn-$(CH_3COO)_2{\cdot}2H_2O$. The solution remained colorless and was stirred at room temperature for 3 h. On concentration of the solution, a white precipitate appeared, which was filtered off and washed with water. Yield: 70%. IR (cm^{-1}): ν_{NH} = 3364; $\nu_{C=O}$ = 1616 (br). ^1H NMR (DMSO-d_6): δ 10.00 (s, br, 1H, NH); 7.25 (s, br, 2H, Ar-H); 7.03 (s, br, 2H, Ar-H); 4.42 (s, 2H, CH_2); 3.51 (s, 3H, NCH_3); 3.11 (m, 1H, CH); 1.19 (t, 6H, CH_3)..

X-ray Crystallography. Single crystal X-ray diffraction data were collected at room temperature (293 K) using graphite monochromated Mo Kα radiation (λ = 0.710 73 Å) on a APEX2 CCD diffractometer for **9** and **12** and using Cu Kα (λ = 1.541 78 Å) on a Siemens AED diffractometer equipped with scintillation counter for **10**, HL^1, and HL^2. Lorentz polarization and absorption corrections were applied.[63,64] Structures were solved by direct methods using SIR97[65] and refined by full-matrix least-squares on all F^2 using SHELXL97[66] implemented in the WingX package.[67] Hydrogen atoms were partly located from Fourier difference maps and partly introduced in idealized positions riding on their carrier atoms. Anisotropic displacement parameters were refined for all non-hydrogen atoms. Table 1 summarizes crystal data and structure determination results. Hydrogen bonds were analyzed with SHELXL97[66] and PARST97,[68] and extensive use was made of the Cambridge Crystallographic Data Centre packages[69,70] for the analysis of crystal packing.

Crystallographic data (excluding structure factors) for HL^1, HL^2, **9**, **10**, and **12** have been deposited with the Cambridge Crystallographic Data Centre as supplementary publications CCDC 829359−829363. Copies of the data can be obtained free of charge on application to CCDC, 12 Union Road, Cambridge CB2 1EZ, U.K. (fax, (+44) 1223-336-033; e-mail, deposit@ccdc.cam.ac.uk).

Potentiometric Measurements. The Mg(II), Mn(II), and Co(II) stock solutions were prepared from $MgCl_2{\cdot}6H_2O$ (Aldrich), $MnCl_2{\cdot}4H_2O$ (Janssen), and anhydrous $CoCl_2$ (Aldrich). Zn(II) stock solution was prepared by dissolving zinc granules (Aldrich) with HCl. Their concentrations were determined using EDTA as a titrant. For Mn(II) and Mg(II), the sodium salt of Eriochrome black T in the presence of triethanolamine and hydroxylamine chloride was used as an indicator, while for Co(II) and Zn(II), titrations were performed in the presence of sodium acetate and hexamethylenetetramine, using xylenol orange as indicator. The Co(II) solutions were prepared and stored under nitrogen to avoid oxidation. Equilibrium constants for protonation and complexation reactions were determined by means of potentiometric measurements, carried out in methanol/water = 9:1 v/v solution at ionic strength 0.1 M KCl and 25 ± 0.1 °C, at pH 2.5−11 under N_2. Temperature was controlled to ±0.1 °C by using a thermostated circulating water bath (ISCO GTR 2000 IIx). Appropriate aliquots of ligand solution, prepared by weight, were titrated with standard KOH (solvent of methanol/water = 9:1 v/v, I = 0.1 M KCl) with and without metal ions, applying constant speed magnetic stirring. Freshly boiled methanol and double-distilled water, kept under N_2, were used throughout. The experimental procedure in order to reach very high accuracy in the determination of the equilibrium constants in this mixed solvent has been described in detail elsewhere.[71] The protonation constants of the ligands were obtained by titrating 20−50 mL samples of each ligand (3×10^{-3} to 9×10^{-3} M). For the complex formation constants, the titrations were performed with different ligand/metal ratios (1 up to 5). At least two measurements (about 60 experimental points each) were performed for each system. Potentiometric titrations were carried out by a fully automated apparatus equipped with a CRISON GLP 21-22 digital voltmeter (resolution, 0.1 mV) and a 5 mL Metrohm Dosimat 655 autoburet, both controlled by a homemade software in BASIC, working on an IBM computer. The electrodic chain (Crison 5250 glass electrode and 0.1 M KCl in methanol/water = 9:1 v/v calomel electrode, Radiometer 401) was calibrated in terms of $[H^+]$ by means of a strong acid−strong base titration by Gran's method,[72] allowing the determination of the standard potential, $E°$ (371.5 ± 0.4 mV), and of the ionic product of water, K_w (pK_w = 14.40 ± 0.05) in the experimental conditions used. The software HYPERQUAD[59] was used to evaluate the protonation and complexation constants from emf data.

Biological Materials, Chemicals, and Enzymes. All compounds were dissolved in DMSO, and the stock solutions were stored at −20 °C. The $\gamma[^{32}P]$ATP was purchased from PerkinElmer. The expression system for wild-type IN was a generous gift of Dr. Robert Craigie, Laboratory of Molecular Biology, NIDDK, NIH, Bethesda, MD.

Preparation of Oligonucleotide Substrates. The oligonucleotides 21top, 5′-GTGTGGAAAATCTCTAGCAGT-3′, and 21bot, 5′-ACTGCTAGAGATTTTCCACAC-3′, were purchased from Norris Cancer Center Core Facility (University of Southern California) and purified by UV shadowing on polyacrylamide gel. To analyze the extent of 3′-processing and strand transfer using 5′-end labeled substrates, 21top was 5′-end labeled using T_4 polynucleotide kinase (Epicentre, Madison, WI) and $\gamma[^{32}P]$ATP (Amersham Biosciences or ICN). The kinase was heat-inactivated, and 21bot was added in 1.5 molar excess. The mixture was heated at 95 °C, allowed to cool slowly to room temperature, and run through a spin 25 minicolumn (USA Scientific) to separate annealed double-stranded oligonucleotide from unincorporated material.

Integrase Assays. To determine the extent of 3′-processing and strand transfer, wild-type IN was preincubated at a final concentration of 200 nM with the inhibitor in reaction buffer (50 mM NaCl, 1 mM HEPES, pH 7.5, 50 μM EDTA, 50 μM dithiothreitol, 10% glycerol (w/v), 7.5 mM $MnCl_2$, 0.1 mg/mL bovine serum albumin, 10 mM 2-mercaptoethanol, 10% DMSO, and 25 mM MOPS, pH 7.2) at 30 °C for 30 min. Then 20 nM of the 5′-end ^{32}P-labeled linear oligonucleotide substrate was added, and incubation was continued for an additional 1 h. Reactions were quenched by the addition of an equal volume (16 μL) of loading dye (98% deionized formamide, 10 mM EDTA, 0.025% xylene cyanol, and 0.025% bromophenol blue). An aliquot (5 μL) was electrophoresed on a denaturing 20% polyacrylamide gel (0.09 M Tris-borate, pH 8.3, 2 mM EDTA, 20% acrylamide, 8 M urea).

Gels were dried, exposed in a PhosphorImager cassette, analyzed using a Typhoon 8610 variable mode imager (Amersham Biosciences), and quantitated using ImageQuant 5.2. Percent inhibition (%I) was calculated using the following equation:

$$\%I = 100 \times [1 - (D - C)/(N - C)]$$

dx.doi.org/10.1021/jm200851g | J. Med. Chem. 2011, 54, 8407−8420

where *C*, *N*, and *D* are the fractions of the 21-mer substrate converted to 19-mer (3′-proc product) or ST products for DNA alone, DNA plus IN, and IN plus drug, respectively. The IC_{50} values were determined by plotting the logarithm of drug concentration versus percent inhibition to obtain the concentration that produced 50% inhibition.

■ ASSOCIATED CONTENT

Supporting Information

Figures S1−S4 illustrating the crystal packing of ligands HL^1 and HL^2 and of complexes **9** and **10**, respectively; Table S1 listing crystal data and structure refinement for compounds HL^1, HL^2, **9**, **10**, and **12**; Table S2 listing elemental analysis data for ligands **2**, **5**, **6**, **8**−**13**, and complexes HL^1 and HL^2. This material is available free of charge via the Internet at http://pubs.acs.org. Crystallographic data (excluding structure factors) for HL^1, HL^2, **9**, **10**, and **12** have been deposited with the Cambridge Crystallographic Data Centre as Supplementary Publications Nos. CCDC 829359−829363. Copies of the data can be obtained free of charge on application to CCDC, 12 Union Road, Cambridge CB2 1EZ, U.K. (fax, (+44) 1223-336-033; e-mail, deposit@ccdc.cam.ac.uk).

■ AUTHOR INFORMATION

Corresponding Author

*Phone: +39 0521 905419. E-mail: dominga.rogolino@unipr.it.

■ ACKNOWLEDGMENTS

The authors thank the "Centro Interfacoltà Misure Giuseppe Casnati" and the "Laboratorio di Strutturistica Mario Nardelli" of the University of Parma, Italy, for facilities. We thank Dr. Maria Orecchioni and Paolo Fiori for assistance with NMR spectroscopy, Dr. Fabrizio Carta for his help on the preparation of the ligand HL^2, and Giuseppe Foroni for technical assistance. M.S. is grateful to Università di Sassari, Italy, for their partial financial support. The work in N.N.'s laboratory was supported by funds from the Campbell Foundation.

■ ABBREVIATIONS USED

HIV-1, human immunodeficiency virus type 1; IN, HIV-1 integrase; DKA, *β*-diketo acid; HPCA, hydroxypyrimidinecarboxamide; QCA, quinolonecarboxylic acid; SSTI, selective strand transfer inhibitor

■ REFERENCES

(1) Pommier, Y.; Johnson, A. A.; Marchand, C. Integrase inhibitors to treat HIV/AIDS. *Nat. Rev. Drug Discovery* **2005**, *4*, 236−248.

(2) Neamati, N. In *HIV-1 Integrase: Mechanism and Inhibitor Design*, Wiley Series on Drug Discovery and Development; Wiley & Sons: New York, 2011.

(3) Dayam, R.; Al-Mawsawi, L. Q.; Neamati, N. HIV-1 integrase inhibitors: an emerging clinical reality. *Drugs R D.* **2007**, *8*, 155−168.

(4) Al-Mawsawi, L. Q.; Al-Safi, R. I.; Neamati, N. Anti-infectives: clinical progress of HIV-1 integrase inhibitors. *Expert. Opin. Emerging Drugs* **2008**, *13*, 213−225.

(5) Vandekerckhove, L. *Curr. Opin. Invest. Drugs* **2010**, *11* (2), 203−212.

(6) MK-0518 Meeting Transcript; Antiviral Drugs Advisory Committee, Center for Drug Evaluation and Research, Department of Health and Human Services, Food and Drug Administration, September 5, 2007; www.fda.gov/ohrms/dockets/ac/cder07.htm#AntiviralDrugs.

(7) Kulkosky, J.; Jones, K. S.; Katz, R. A.; Mack, J. P.; Skalka, A. M. Residues critical for retroviral integrative recombination in a region that is highly conserved among retroviral/retrotransposon integrases and bacterial insertion sequence transposases. *Mol. Cell. Biol.* **1992**, *12*, 2331−2338.

(8) Chiu, T. K.; Davies, D. R. Structure and function of HIV Integrase. *Curr. Top. Med. Chem.* **2004**, *4*, 965−979.

(9) Kirschberg, T.; Parrish, J. Metal chelators as antiviral agents. *Curr. Opin. Drug Discovery* **2007**, *10*, 460−472.

(10) Rouffet, M.; Cohen, S. M. Emerging trends in metalloprotein inhibition. *Dalton Trans.* **2011**, *40*, 3445.

(11) Pais, G. C. G.; Burke, T. R. Novel aryl diketo-containing inhibitors of HIV-1 integrase. *Drugs Future* **2002**, *27*, 1101−1111.

(12) Dayam, R.; Sanchez, T.; Neamati, N. Diketo acid pharmacophore. 2. Discovery of structurally diverse inhibitors of HIV-1 integrase. *J. Med. Chem.* **2005**, *48*, 8009−8015.

(13) Kawasuji, T.; Yoshinaga, T.; Sato, A.; Yodo, M.; Fujiwara, T.; Kiyama, R. A platform for designing HIV integrase inhibitors. Part 1: 2-Hydroxy-3-heteroaryl acrylic acid derivatives as novel HIV integrase inhibitor and modeling of hydrophilic and hydrophobic pharmacophores. *Bioorg. Med. Chem.* **2006**, *14*, 8430−8445.

(14) Dayam, R.; Neamati, N. Active site binding modes of the beta-diketoacids: a multi-active site approach in HIV-1 integrase inhibitor design. *Bioorg. Med. Chem.* **2004**, *12*, 6371−6381.

(15) Pais, G. C. G.; Zhang, X.; Marchand, C.; Neamati, N.; Cowansage, K.; Svarovskaia, E. S.; Pathak, V. K.; Tang, Y.; Nicklaus, M.; Pommier, Y.; Burke, T. R. Jr. Structure activity of 3-aryl-1,3-diketo-containing compounds as HIV-1 integrase inhibitors. *J. Med. Chem.* **2002**, *45*, 3184−3194.

(16) Zhao, X. Z.; Maddali, K.; Vu, B. C.; Marchand, C.; Hughes, S. H.; Pommier, Y.; Burke, T. R. Jr. Examination of halogen substituent effects on HIV-1 integrase inhibitors derived from 2,3-dihydro-6,7-dihydroxy-1*H*-isoindol-1-ones and 4,5-dihydroxy-1*H*-isoindole-1,3(2*H*)-diones. *Bioorg. Med. Chem. Lett.* **2009**, *19*, 2714−2717.

(17) Egbertson, M. S. HIV integrase inhibitors: from diketoacids to heterocyclic templates: a history of HIV integrase medicinal chemistry at Merck West Point and Merck Rome (IRBM). *Curr. Top. Med. Chem.* **2007**, *7*, 1251−1272.

(18) Billich, A. S-1360 Shionogi-GlaxoSmithKline. *Curr. Opin. Invest. Drugs* **2003**, *4*, 206−209.

(19) Garvey, E. P.; Johns, B. A.; Gartland, M. J.; Foster, S. A.; Miller, W. H.; Ferris, R. G.; Hazen, R. J.; Underwood, M. R.; Boros, E. E.; Thompson, J. B.; Weatherhead, J. G.; Koble, C. S.; Allen, S. H.; Schaller, L. T.; Sherrill, R. G.; Yoshinaga, T.; Kobayashi, M.; Wakasa-Morimoto, C.; Miki, S.; Nakahara, K.; Noshi, T.; Sato, A.; Fujiwara, T. The naphthyridinone GSK364735 is a novel, potent human immunodeficiency virus type 1 integrase inhibitor and antiretroviral. *Antimicrob. Agents Chemother.* **2008**, *52*, 901−908.

(20) Boros, E. E.; Edwards, C. E.; Foster, S. A.; Fuji, M.; Fujiwara, T.; Garvey, E. P.; Golden, P. L.; Hazen, R. J.; Jeffrey, J. L.; Johns, B. A.; Kawasuji, T.; Kiyama, R.; Koble, C. S.; Kurose, N.; Miller, W. H.; Mote, A. L.; Murai, H.; Sato, A.; Thompson, J. B.; Woodward, M. C.; Yoshinaga, T. Synthesis and antiviral activity of 7-benzyl-4-hydroxy-1,5-naphthyridin-2(1*H*)-one HIV integrase inhibitors. *J. Med. Chem.* **2009**, *52*, 2754−2761.

(21) Wang, Y.; Serradell, N.; Bolos, J.; Rosa, E. MK-0518, HIV integrase inhibitor. *Drugs Future* **2007**, *32*, 118−122.

(22) Rowley, M. The discovery of raltegravir, an integrase inhibitor for the treatment of HIV infection. *Prog. Med. Chem.* **2008**, *46*, 1−28.

(23) Summa, V.; Petrocchi, A.; Bonelli, F.; Crescenzi, B.; Donghi, M.; Ferrara, M.; Fiore, F.; Gardelli, C.; Gonzalez, P. O.; Hazuda, D. J.; Jones, P.; Kinzel, O.; Laufer, R.; Monteagudo, E.; Muraglia, E.; Nizi, E.; Orvieto, F.; Pace, P.; Pescatore, G.; Scarpelli, R.; Stillmock, K.; Witmer, M. V.; Rowley, M. Discovery of raltegravir, a potent, selective orally bioavailable HIV-integrase inhibitor for the treatment of HIV-AIDS infection. *J. Med. Chem.* **2008**, *51*, 5843−5855.

(24) Markowitz, M.; Morales-Ramirez, J. O.; Nguyen, B.-Y.; Kovacs, C. M.; Steigbigel, R. T.; Cooper, D. A.; Liporace, R.; Schwartz, R.; Isaacs, R.; Gilde, L. R.; Wenning, L.; Zhao, J.; Teppler, H. Antiretroviral activity, pharmacokinetics, and tolerability of MK-0518, a novel inhibitor of HIV-1 integrase, dosed as monotherapy

for 10 days in treatment-naive HIV-1-infected individuals. *J. Acquired Immune Defic. Syndr.* **2006**, *43*, 509−515.
(25) Sato, M.; Motomura, T.; Aramaki, H.; Matsuda, T.; Yamashita, M.; Ito, Y.; Kawakami, H.; Matsuzaki, Y.; Watanabe, W.; Yamataka, K.; Ikeda, S.; Kodama, E.; Matsuoka, M.; Shinkai, H. Novel HIV-1 integrase inhibitors derived from quinolone antibiotics. *J. Med. Chem.* **2006**, *49*, 1506−1508.
(26) Dayam, R.; Al-Mawsawi, L. Q.; Zawahir, Z.; Witvrouw, M.; Debyser, Z.; Neamati, N. Quinolone 3-carboxylic acid pharmacophore: design of second generation HIV-1 integrase inhibitors. *J. Med. Chem.* **2008**, *51*, 1136−1144.
(27) Pasquini, S.; Mugnaini, C.; Tintori, C.; Botta, M.; Trejos, A.; Arvela, R. K.; Larhed, M.; Witvrouw, M.; Michiels, M.; Christ, F.; Debyser, Z.; Corelli, F. Investigations on the 4-quinolone-3-carboxylic acid motif. 1. Synthesis and structure−activity relationship of a class of human immunodeficiency virus type 1 integrase inhibitors. *J. Med. Chem.* **2008**, *51*, 5125−5129.
(28) DeJesus, E.; Berger, D.; Markovitz, M.; Cohen, C.; Hawkins, T.; Ruane, P.; Elion, R.; Farthing, C.; Zhong, L.; Cheng, A. K.; McKoll, D.; Kearney, B. P. Antiviral activity, pharmacokinetics, and dose response of the HIV-1 integrase inhibitor GS-9137 (JTK-303) in treatment-naive and treatment-experienced patients. *J. Acquired Immune Defic. Syndr.* **2006**, *43*, 1−5.
(29) Kobayashi, M.; Yoshinaga, T; Seki, T.; Wakasa-Morimoto, C.; Brown, K. W.; Ferris, R.; Foster, S. A.; Hazen, R. J.; Miki, S.; Suyama-Kagitani, A.; Kawauchi-Miki, S.; Taishi, T.; Kawasuji, T.; Johns, B. A.; Underwood, M. R.; Garvey, E. P.; Sato, A.; Fujiwara, T. In vitro antiretroviral properties of S/GSK1349572, a next-generation HIV Integrase inhibitor. *Antimicrob. Agents Chemother.* **2011**, *55*, 813−821.
(30) Kiyama, R.; Kawasuji, T. PCT Int. Appl. WO-01/95905, 2001.
(31) Johns, B. A.; Svolto, A. C. Advances in two-metal chelation inhibitors of HIV integrase. *Expert Opin. Ther. Pat.* **2008**, *18*, 1225−1237.
(32) Hare, S.; Gupta, S. S.; Valkov, E.; Engelman, A.; Cherepanov, P. Retroviral intasome assembly and inhibition of DNA strand transfer. *Nature* **2010**, *464*, 232−236.
(33) Sechi, M.; Bacchi, A.; Carcelli, M.; Compari, C.; Duce, E.; Fisicaro, E.; Rogolino, D.; Gates, P.; Derudas, M.; Al-Mawsawi, L. Q.; Neamati, N. From ligand to complexes: inhibition of human immunodeficiency virus type 1 integrase by β-diketo acid metal complexes. *J. Med. Chem.* **2006**, *49*, 4248−4260.
(34) Bacchi, A.; Biemmi, M.; Carcelli, M.; Carta, F.; Compari, C.; Fisicaro, E.; Rogolino, D.; Sechi, M.; Sippel, M.; Sotriffer, C.; Sanchez, T. W.; Neamati, N. From ligand to complexes. Part 2. Remarks on human immunodeficiency virus type 1 integrase inhibition by β-diketo acid metal complexes. *J. Med. Chem.* **2008**, *51*, 7253−7264.
(35) Maurin, C.; Bailly, F.; Buisine, E.; Vezin, H.; Mbemba, G.; Mouscadet, J. F.; Cotelle, P. Spectroscopic studies of diketoacids−metal interactions. A probing tool for the pharmacophoric intermetallic distance in the HIV-1 integrase active site. *J. Med. Chem.* **2004**, *47*, 5583−5596.
(36) Mitscher, L. A. Bacterial topoisomerase inhibitors: quinolone and pyridone antibacterial agents. *Chem. Rev.* **2005**, *105*, 559−592.
(37) Brighty, K. E.; Gootz, T. D. *The Quinolones*; Andriole, V.T., Ed.; Academic Press: San Diego, CA, 2000; pp 33−97 .
(38) Laponogov, I.; Sohi, M. K.; Veselkov, D. A.; Pan, X. S.; Sawhney, R.; Thompson, A. W.; McAuley, K. E.; Fisher, L. M.; Sanderson, M. R. Structural insight into the quinolone−DNA cleavage complex of type IIA topoisomerases. *Nat. Struct. Biol.* **2009**, *16*, 667−669.
(39) Turel, I. The interactions of metal ions with quinolone antibacterial agents. *Coord. Chem. Rev.* **2002**, *232*, 27−47.
(40) Sadeek, S. A. Synthesis, thermogravimetric analysis, infrared, electronic and mass spectra of Mn(II), Co(II), and Fe(III) norfloxacin complexes. *J. Mol. Struct.* **2005**, *753*, 1−12.
(41) Drevenšek, P.; Košmrlj, J.; Giester, G.; Skauge, T.; Sletten, E.; Sepčić, K; Turel, I. X-ray crystallographic, NMR and antimicrobial activity studies of magnesium complexes of fluoroquinolones—racemic ofloxacin and its *S*-form, levofloxacin. *J. Inorg. Biochem.* **2006**, *100*, 1755−1763.
(42) Turel, I.; Živec, P.; Pevec, A.; Tempelaar, S; Psomas, G. Compounds of antibacterial agent ciprofloxacin and magnesium—crystal structures and molecular modeling calculations. *Eur. J. Inorg. Chem.* **2008**, 3718−3727.
(43) Lecomte, S.; Baron, M. H.; Chenon, M. T.; Coupry, C.; Moreau, N. J. Effect of magnesium complexation by fluoroquinolones on their antibacterial properties. *Antimicrob. Agents Chemother.* **1994**, *38*, 2810−2816.
(44) Chen, I. J.; Neamati, N.; MacKerell, A. D. Jr. Structure-based inhibitor design targeting HIV-1 integrase. *Curr. Drug Targets: Infect. Disord.* **2002**, *2*, 217−234.
(45) Maurin, C.; Bailly, F.; Cotelle, P. Structure−activity relationships of HIV-1 integrase inhibitors: enzyme−ligand interactions. *Curr. Med. Chem.* **2003**, *10*, 1795−1810.
(46) Drevenšek, P.; Turel, I.; Poklar Ulrih, N. Influence of copper(II) and magnesium(II) ions on the ciprofloxacin binding to DNA. *J. Inorg. Biochem.* **2003**, *96*, 407−415.
(47) Jimenez-Garrido, N.; Perello, L.; Ortiz, R.; Alzuet, G.; Gonzalez-Alvarez, M; Canton, E.; Liu-Gonzalez, M.; Garcia-Granada, S.; Perez-Priede, M. Antibacterial studies, DNA oxidative cleavage, and crystal structures of Cu(II) and Co(II) complexes with two quinolone family members, ciprofloxacin and enoxacin. *J. Inorg. Biochem.* **2005**, *99*, 677−689.
(48) Katsarou, M. E.; Efthimiadou, E. K.; Psomas, G.; Karaliota, A.; Vourloumis, D. Novel copper(II) complex of *N*-propyl-norfloxacin and 1,10-phenanthroline with enhanced antileukemic and DNA Nuclease activities. *J. Med. Chem.* **2008**, *51*, 470−478.
(49) Tarushi, A.; Psomas, G..; Raptopoulou, C. P.; Kessissoglou, D. P. Zinc complexes of the antibacterial drug oxolinic acid: structure and DNA-binding properties. *J. Inorg. Biochem.* **2009**, *103*, 898−905.
(50) Psomas, G.; Tarushi, A.; Efthimiadou, E. K.; Sanakis, Y.; Raptopoulou, C. P.; Katsaros, N. Synthesis, structure and biological activity of copper(II) complexes with oxolinic acid. *J. Inorg. Biochem.* **2006**, *100*, 1764−1773.
(51) Okabayashi, Y.; Hayashi, F.; Terui, Y.; Kitagawa, T. Studies on the interaction of pyridone carboxylic acids with metals. *Chem. Pharm. Bull.* **1992**, *40*, 692−296.
(52) Chen, Z.-F.; Xiong, R.-G.; Zuo, J.-L.; Guo, Z.; You, X.-Z.; Fun, H.-K. X-ray crystal structures of Mg^{2+} and Ca^{2+} dimers of the bacterial drug norfloxacin. *J. Chem. Soc., Dalton Trans.* **2000**, 4013−4014.
(53) Wang, Y.-C.; Zhao, H.; Ye, Q.; Chen, Z.-F.; Xiong, R.-G.; Fun, H.-K. Novel supramolecular array based on antibacterial drug norfloxacin. *Inorg. Chim. Acta* **2004**, *357*, 4303−4308.
(54) Xiao, D.-R.; Wang, E.-B.; An, H.-Y.; Su, Z.-M.; Li, Y.-G.; Gao, L.; Sun, C.-Y.; Xu, L. Rationally designed, polymeric, extended metal−ciprofloxacin complexes. *Chem.—Eur. J.* **2005**, *11*, 6673−6686.
(55) Sunderland, C. J.; Botta, M.; Aime, S.; Raymond, K. N. 6-Carboxamido-5,4-hydroxypyrimidinones: a new class of heterocyclic ligands and their evaluation as gadolinium chelating agents. *Inorg. Chem.* **2001**, *40*, 6746−6756.
(56) Nakamoto, K. *Infrared and Raman Spectra of Inorganic and Coordination Compounds*, 4th ed.; Wiley: New York, 1986.
(57) Deacon, G. B.; Phillips, R. J. Relationships between the carbon−oxygen stretching frequencies of carboxylato complexes and the type of carboxylate coordination. *Coord. Chem. Rev.* **1980**, *33*, 227−250.
(58) Bruno, I. J.; Cole, J. C.; Kessler, M.; Luo, Jie; Motherwell, W. D. S.; Purkis, L. H.; Smith, B. R.; Taylor, R.; Cooper, R. I.; Harris, S. E.; Orpen, A. G. Retrieval of crystallographically-derived molecular geometry information. *J. Chem. Inf. Comput. Sci.* **2004**, *44*, 2133−2144.
(59) Bacchi, A.; Carcelli, M.; Compari, C.; Fisicaro, E.; Pala, N.; Rispoli, G.; Rogolino, D.; Sanchez, T. W.; Sechi, M.; Neamati, N. HIV-1 IN strand-tranfer chelating inhibitors: a focus on metal binding. *Mol. Pharmaceutics* **2011**, *8* (2), 507−519.
(60) Gans, P.; Sabatini, A.; Vacca, A. Investigation of equilibria in solution. Determination of equilibrium constants with the HYPERQUAD suite of programs. *Talanta* **1996**, *43*, 1739−1753.

(61) Irving, H.; Williams, R. J. P. Order of stability of metal complexes. *Nature* **1948**, *162*, 746−747.
(62) Wohlkonig, A.; Chan, P. F.; Fosberry, A. P.; Homes, P.; Huang, J.; Kranz, M.; Leydon, V. R.; Miles, T. J; Pearson, N. D.; Perera, R. L.; Shillings, A. J.; Gwynn, M. N.; Bax, B. D. Structural basis of quinolone inhibition of type IIA topoisomerases and target-mediated resistance. *Nat. Struct. Mol. Biol.* **2010**, *17*, 1152−1153.
(63) *SAINT: SAX, Area Detector Integration*; Siemens Analytical Instruments Inc.: Madison, WI, U.S.
(64) Sheldrick, G. *SADABS: Siemens Area Detector Absorption Correction Software*; University of Goettingen: Goettingen, Germany1996.
(65) Altomare, A.; Burla, M. C.; Camalli, M.; Cascarano, G.; Giacovazzo, C.; Guagliardi, A.; Moliterni, A. G.; Polidori, G.; Spagna, R. *Sir97: A New Program for Solving and Refining Crystal Structures*; Istituto di Ricerca per lo Sviluppo di Metodologie Cristallografiche CNR: Bari, Italy. 1997.
(66) Sheldrick, G. *SHELXL97. Program for Structure Refinement*; University of Goettingen: Goettingen, Germany, 1997.
(67) Farrugia, L. J. WinGX suite for small-molecule single-crystal crystallography. *J. Appl. Crystallogr.* **1999**, *32*, 837−838.
(68) Nardelli, M. PARST95—an update to PARST: a system of Fortran routines for calculating molecular structure parameters from the results of crystal structure analyses. *J. Appl. Crystallogr.* **1995**, *28*, 659.
(69) Allen, F. H.; Kennard, O.; Taylor, R. Systematic analysis of structural data as a research technique in organic chemistry. *Acc. Chem. Res.* **1983**, *16*, 146−153.
(70) Bruno, I. J.; Cole, J. C.; Edgington, P. R.; Kessler, M.; Macrae, C. F.; McCabe, P.; Pearson, J.; Taylor, R. New software for searching the Cambridge Structural Database and visualizing crystal structures. *Acta Crystallogr.* **2002**, *B58*, 389−397.
(71) Fisicaro, E.; Braibanti, A. Potentiometric titrations in methanol/water medium. *Talanta* **1988**, *10*, 769−774.
(72) Gran, G. Determination of the equivalence point in potentiometric titrations. Part II. *Analyst* **1952**, *77*, 661−671.